石井賢二	アミロイドイメージングの現状と有用性	神経内科	77(6)	597-605	2012
石井賢二	認知症の画像診断	医薬ジャーナル	48(8)	1973-1977	2012
石井賢二	PETを用いた新しい脳機能診断	Rad Fan	10(12)	48-50	2012
石井賢二	アミロイドイメージングとアルツハイマー病の発症予測・予防研究	Medical Science Digest	38(10)	432-435	2012
石井賢二	精神疾患の生物学的検査法の近未来　アミロイドPET	臨床精神医学	41(7)	863-869	2012
石井賢二	Preclinical stageのアミロイドイメージングから期待されるもの	老年精神医学雑誌	23(6)	693-700	2012
石井賢二	画像検査から見た認知症疾患の鑑別診断	最新医学	31(4)	767-774	2012
石井賢二	認知症診断におけるマルチモーダルアプローチ：アミロイドPETとFDG-PETによる認知症診断	Cognition and Dementia	11(2)	14-20	2012
嶋田裕之	糖尿病があると認知症になりやすいって本当？	糖尿病ケア	9	69-72	2012
嶋田裕之	高齢者タウオパチー（嗜銀顆粒性認知症、神経原線維変化型認知症）の臨床	日本老年医学会雑誌	49	281-283	2012
三木隆己	アミロイドペット検査の臨床的有用性	老年期認知症研究会誌	19	89-91	2012
篠遠 仁	脳機能画像からみたリバスチグミンの効果	脳21	15(2)	166-172	2012
伊藤 浩，島田 斉	PET - 認知症	映像情報メディカル	44(7)	674-681	2012
篠遠 仁	アセチルコリンと神経系　記憶	Clinical Neuroscience	30(2)	128-129	2012
篠遠 仁	コリン作動性シナプスのイメージング	Clinical Neuroscience	30(6)	675-678	2012
篠遠 仁，平野成樹	CBSにおける画像診断	BRAIN and NERVE	65(1)	41-53	2013
平野成樹，島田 斉，吉山容正	糖尿病と脳画像研究 アルツハイマー病発症機序との関連を考える	BRAIN and NERVE	64(12)	1411-1419	2012
樋口真人	認知症のバイオマーカーイメージング	Cognition and Dementia	12(1)	34-40	2013
樋口真人	画像・バイオマーカーによるアルツハイマー病の早期診断	カレントテラピー	30(4)	306-313	2012
伊藤健吾，加藤隆司	脳血流と脳糖代謝所見はpreclinical stageの診断に役立つか	老年精神医学雑誌	23	701-707	2012
伊藤健吾，藤原 謙，加藤隆司	アルツハイマー病に関する多施設共同研究．特集　アルツハイマー病の診断と治療の最前線．	PETジャーナル	(19)	16-18	2012
加藤隆司，簇野健太郎，伊藤健吾	アルツハイマー病診断の新しい展開 特集　核医学検査の効果的な活用法　～最先端の技術を学ぶ	映像情報Medical	(11):	890-895	2012
百瀬敏光	診療に役立つ核医学の基本　「脳神経核医学　臨床編その1」	臨床核医学	46-1	8-12	2013
百瀬敏光	診療に役立つ核医学の基本　「脳神経核医学　臨床編その2」	臨床核医学	46-2	23-26	2013
高尾昌樹	軽度認知障害の神経病理学	臨床神経学	52	851-854	2012
高尾昌樹	脳表ヘモシデリン沈着症とNeuroferritinopathyの神経病理	臨床神経学	52	959-961	2012
今林悦子	特集3　PET薬剤と合成装置の進歩 3)核医学からみたアミロイドーシス	PET　Journal	20	36-38	2012

6. 邦文単行本

著者名	論文題名	書名	編集者名	出版社名	出版地	頁	出版年
石井賢二	認知症や軽度認知障害診断におけるアミロイドPETの臨床的意義	認知症診療Q&A92	中島健二,和田健二編	中外医学社	東京	291-293	2012
三木隆己，嶋田裕之	消化器疾患に伴う骨粗鬆症胃切除	骨粗鬆症診療ハンドブック　改訂5版		医薬ジャーナル社		77-81	
三木隆己，嶋田裕之	活性型ビタミンD3製剤編 男性骨粗鬆症	ファーマーナビゲーター		メディカルレビュー社		130-137	
篠遠 仁	SPECTによる神経伝達機能の測定 2.ドパミン・トランスポータ	脳SPECT/PETの臨床	西村恒彦	(株)メジカルビュー社		117-125	2012
新井憲俊，横地房子，大西 隆，百瀬敏光，沖山亮一，谷口 真，高橋 宏，松田博史，宇川義一	一側の視床下核刺激でも両側の症状の改善をみる機序について：PETを用いた研究	ジストニア2012	長谷川一子 編	中外医学社	東京	228-230	2012
百瀬敏光	PET装置による分子イメージングと放射免疫療法の開発	新機能抗体開発ハンドブック	浜窪隆雄 監	NYS	東京	369-37	2012
荒井拓也，百瀬敏光	ラジオアイソトープによるモノクローナル抗体の標識	新機能抗体開発ハンドブック	浜窪隆雄 監	NYS	東京	374-378	2012
北田孝幸，百瀬敏光	PET/SPECTを用いたin vivoイメージング技術	新機能抗体開発ハンドブック	浜窪隆雄 監	NYS	東京	379-382	2012
百瀬敏光	神経伝達機能イメージング	Annual Review 神経2013	鈴木則宏, 他編	中外医学社	東京	51-62	2013
百瀬敏光，高橋美和子	間脳・下垂体の核医学検査	ビジュアル脳神経外科6 間脳・下垂体・傍鞍部	斉藤延人 編	メジカルビュー社	東京	80－91	2013

Ⅴ. 研究成果の刊行物・別刷

Amyloid Imaging Mismatch

Ryogo Minamimoto, MD, PhD, Kenji Ishii, MD, PhD,† Kazuo Kubota, MD, PhD,* Miyako Morooka, MD, PhD,* Momoko Okasaki, MD,* Kimiteru Ito, MD, PhD,‡ Takuya Mitsumoto, MSc,* Kazuhiko Nakajima,* Takashi Sato,* Makoto Mochizuki, MD, PhD,§ and Osamu Okazaki, MD, PhD||*

Abstract: An 82-year-old man with suspected systemic amyloidosis and complete atrioventricular block underwent vascular biopsy during his pacemaker implantation with pathology showing amyloid deposits. ^{99m}Tc-aprotinin SPECT revealed increased radiotracer uptake along the left ventricular wall, consistent with cardiac amyloidosis. ^{11}C-PiB PET/CT performed for the evaluation of amyloid deposits in the brain showed findings suggestive of Alzheimer disease without abnormal radiotracer concentration in the myocardium to match the ^{99m}Tc-aprotinin SPECT findings. Dynamic PET images showed increased ^{11}C-PiB concentration in the left ventricular myocardium at 2 minutes after injection, with subsequent tracer clearance by approximately 5 minutes, consistent with normal ^{11}C-PiB biodistribution.

Key Words: amyloidosis, ^{99m}Tc-aprotinin, ^{11}C-PiB, Alzheimer disease, amyloid imaging

(*Clin Nucl Med* 2012;37: 807–809)

Received for publication October 13, 2011; and revision accepted February 21, 2012.

From the *Division of Nuclear Medicine, Department of Radiology, National Center for Global Health and Medicine; †Positron Medical Center, Tokyo Metropolitan Institute of Gerontology; ‡Department of Radiology, National Center of Neurology and Psychiatry; and §Division of Pathology, Departments of Central Laboratory and ||Cardiology, National Center for Global Health and Medicine, Tokyo, Japan.

This work was supported by a grant from the National Center for Global Health and Medicine (no. 22-118 to Dr Minamimoto).

Reprints: Ryogo Minamimoto, MD, PhD, Division of Nuclear Medicine, Department of Radiology, National Center for Global Health and Medicine, 1-21-1, Toyama, Shinjyuku-ku, Tokyo 162-8655, Japan. E-mail: ryogominamimoto@yahoo.co.jp.

ISSN: 0363-9762/12/3708-0807

REFERENCES

1. Sojan SM, Smyth DR, Tsopelas C, et al. Pharmacokinetics and normal scintigraphic appearance of ^{99m}Tc aprotinin. *Nucl Med Commun.* 2005;26: 535–539.
2. Cardoso I, Pereira PJ, Damas AM, et al. Aprotinin binding to amyloid fibrils. *Eur J Biochem.* 2000;267:2307–2311.
3. Aprile C, Marinone G, Saponaro R, et al. Cardiac and pleuropulmonary AL amyloid imaging with technetium-99m labeled aprotinin. *Eur J Nucl Med.* 1995;22:1393–1401.
4. Han S, Chong V, Murray T, et al. Preliminary experience of ^{99m}Tc-aprotinin scintigraphy in amyloidosis. *Eur J Haematol.* 2007;79:494–500.
5. Schaadt BK, Hendel HW, Gimsing P, et al. ^{99m}Tc-aprotinin scintigraphy in amyloidosis. *J Nucl Med.* 2003;44:177–183.
6. Glaudemans AW, Slart RH, Zeebregts CJ, et al. Nuclear imaging in cardiac amyloidosis. *Eur J Nucl Med Mol Imaging.* 2009;36:702–714.
7. Nordberg A. PET imaging of amyloid in Alzheimer's disease. *Lancet Neurol.* 2004;3:519–527.
8. Hardy J, Selkoe DJ. The amyloid hypothesis of Alzheimer's disease: progress and problems on the road to therapeutics. *Science.* 2002;297:353–356.
9. Scheinin NM, Tolvanen TK, Wilson IA, et al. Biodistribution and radiation dosimetry of the amyloid imaging agent ^{11}C-PIB in humans. *J Nucl Med.* 2007;48:128–133.
10. Husby G. Nomenclature and classification of amyloid and amyloidoses. *J Intern Med.* 1992;232:511–512.
11. Falk RH, Comenzo RL, Skinner M. The systemic amyloidoses. *N Engl J Med.* 1997;337:898–909.

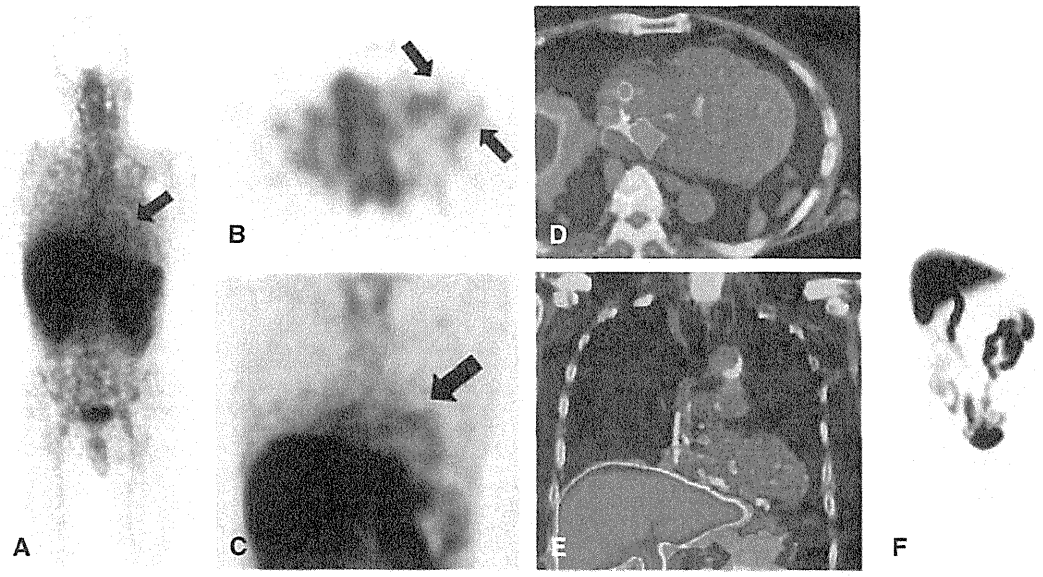

FIGURE 1. An 82-year-old man with complete heart block underwent a vascular biopsy, which showed amyloid deposits. The type of amyloidosis could not be clearly defined by the vascular specimen; however, the patient also complained of progressive memory loss, and systemic amyloidosis was suspected. ^{99m}Tc-aprotinin SPECT images obtained 90 minutes after injection of 740 MBq of ^{99m}Tc-aprotinin revealed abnormal tracer uptake along the left ventricular wall suggestive of cardiac amyloidosis [MIP (A), axial (B), and coronal (C) images]. An ^{11}C-labeled Pittsburgh compound B (^{11}C-PiB) PET/CT was also requested for the evaluation of his memory loss and possible amyloid deposits in the brain. Whole-body PET/CT scans obtained 70 minutes after injection of 740 MBq of ^{11}C-PiB showed no abnormal myocardial uptake in the left ventricular wall to match the ^{99m}Tc-aprotinin SPECT findings [PET/CT fused axial (D), PET/CT fused coronal (E), and MIP (F) images]. Dynamic PET images obtained during the first 40 minutes after ^{11}C-PiB injection show ^{11}C-PiB retention in the left ventricular wall during the first 2 minutes of tracer injection, followed by a relatively rapid washout and subsequent clearance from the myocardial wall by approximately 5 minutes after injection. Antiproteases are known to be present in certain types of amyloid deposits. The proteinase inhibitor aprotinin (Trasylol) is a basic pancreatic trypsin inhibitor.[1] When labeled with ^{99m}Tc, aprotinin is useful for in vivo imaging of amyloid deposits.[2] The tracer was first evaluated by Aprile et al[3] for imaging amyloid deposits in patients with amyloid light chain–type amyloidosis. Currently, ^{99m}Tc-aprotinin is being used for detecting extra-abdominal amyloid deposits, particularly cardiac amyloidosis.[4–6] The PET tracer ^{11}C-PiB is a thioflavin-T derivative and specifically binds to fibrillar amyloid-β plaques originating from the amyloid precursor protein,[7] which is specific to Alzheimer disease.[8] ^{11}C-PiB has a relatively long residence time in the liver and kidneys, being excreted in bile and urine. In contrast, it has a short residence time in the heart.[9] Thus, the short retention time of ^{11}C-PiB in the heart wall confirmed in this case was most consistent with a normal biodistribution. Our results suggest that ^{11}C-PiB may not have sufficient selectivity for the detection of systematic amyloidosis, being rather unsuitable for cardiac imaging.

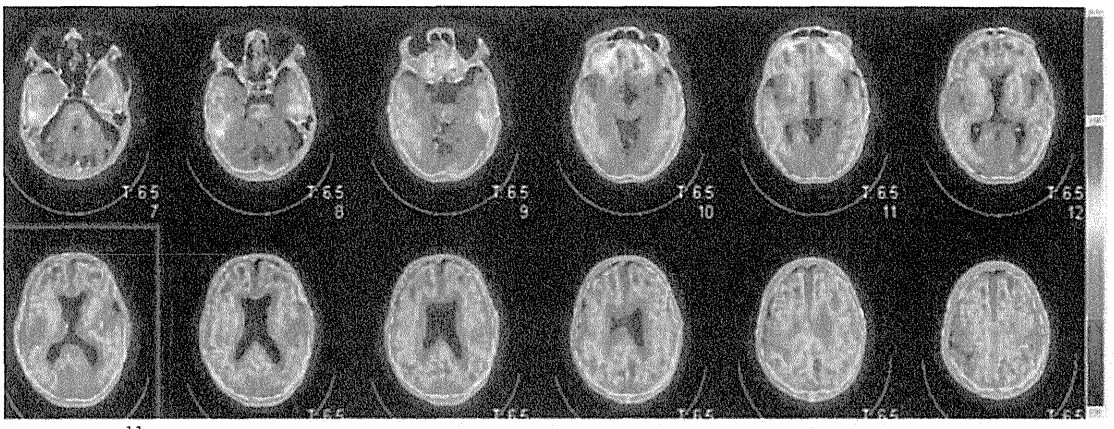

FIGURE 2. Increased ^{11}C-PiB uptake indicating amyloid deposits was noted in the bilateral precuneus, the lateral aspect of both parietotemporal lobes, the frontal cortex, and the ventral striatum. In contrast, no brain uptake was noted on ^{99m}Tc-aprotinin SPECT images; however, this was an expected finding because ^{99m}Tc-aprotinin does not cross the blood-brain barrier.[4] Amyloidosis is a disease caused by extracellular deposition of the amyloid protein and can lead to organ dysfunction and death. Because amyloid deposition can vary in various tissues, the clinical presentation can similarly vary.[10,11] For example, the manifestation of cardiac amyloidosis can vary from myocardial infiltration with amyloid cardiomyopathy to small vessel involvement with cardiac ischemia. In this situation, noninvasive imaging techniques play a significant role in early diagnosis, enabling early interventions and subsequent disease monitoring. However, as our results indicate, selective use of radiopharmaceuticals is also important and should be based on clinical symptoms.

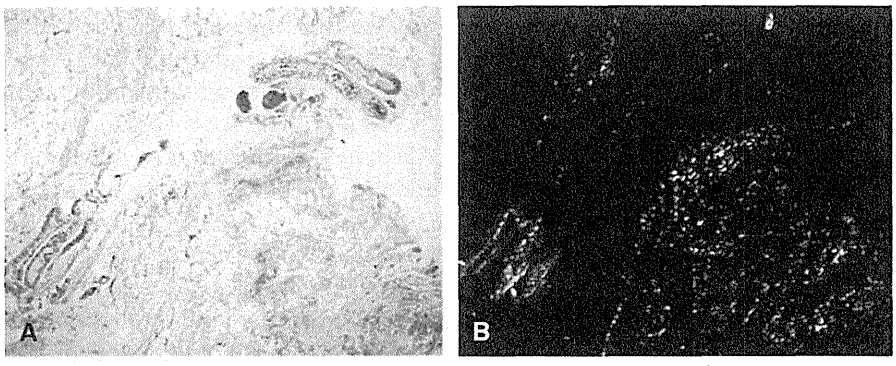

FIGURE 3. Pathological specimen of the vascular connective tissue obtained during pacemaker implantation. A, Pathological specimen demonstrating amyloid deposition (red orange) with Congo red staining. B, Congo red–stained amyloid is also visualized as red-green birefringence with a polarized light.

Original Research Article

Dementia
and Geriatric
Cognitive Disorders

Dement Geriatr Cogn Disord 2012;34:112–120
DOI: 10.1159/000341577

Accepted: June 20, 2012
Published online: September 4, 2012

Clinical Features of Pittsburgh Compound-B-Negative Dementia

Jun Takeuchi[a] Hiroyuki Shimada[a] Suzuka Ataka[a] Joji Kawabe[b]
Hiroshi Mori[c] Kei Mizuno[e] Yasuhiro Wada[e] Susumu Shiomi[b]
Yasuyoshi Watanabe[d,e] Takami Miki[a]

Departments of [a]Geriatrics and Neurology, [b]Nuclear Medicine, [c]Neuroscience and [d]Physiology, Osaka City University Graduate School of Medicine, Osaka, and [e]RIKEN Center for Molecular Imaging Science, Kobe, Japan

Key Words
Alzheimer's disease · Biomarkers · Cerebrospinal fluid biomarkers · FDG-PET · ^{123}I-MIBG myocardial scintigraphy · MRI · Pittsburgh compound B · Tauopathy · Voxel-based morphometry

Abstract
Background/Aims: We previously found that some cases of clinically diagnosed Alzheimer's disease (AD) were rated as Pittsburgh compound B (PiB) negative by amyloid imaging (i.e. cases of PiB-negative dementia). The present study was designed to analyze the clinical features of PiB-negative dementia patients in detail. ***Methods:*** Of the 64 cases of clinically diagnosed AD, 14 were rated PiB negative. Eleven of these were further analyzed using CSF biomarker levels and findings from MRI, FDG-PET, ^{123}I-MIBG myocardial scintigraphy and voxel-based morphometry (VBM). ***Results:*** When examined by ^{123}I-MIBG myocardial scintigraphy, the heart/mediastinum ratio was significantly higher in the PiB-negative dementia group than in the dementia with Lewy bodies (DLB) group. Analyses of CSF biomarkers and MRI and FDG-PET findings suggested argyrophilic grain disease (AGD) in 3 cases, frontotemporal lobar degeneration (FTLD) in 3 cases, neurofibrillary tangle-predominant dementia (NFTD) in 1 case, and AD in 2 cases. In the VBM data analysis, the PiB-positive AD group showed significant atrophy of both hippocampi compared with the healthy control group, while the PiB-negative dementia group presented with significant atrophy of the left precuneus. ***Conclusion:*** PiB-negative dementia is unlikely to include DLB, while it most likely includes diseases of tauopathy, such as FTLD, AGD and NFTD. A better understanding of PiB-negative dementia is expected to further improve the accuracy of the clinical AD diagnosis.

Introduction

The major pathological features of Alzheimer's disease (AD) are senile plaques, which primarily consist of amyloid-β (Aβ) protein, and neurofibrillary tangles, which primarily consist of phosphorylated tau (p-tau). Pittsburgh compound B (PiB), which binds to Aβ protein, is a compound with more advanced clinical applications than any other amyloid imaging agent. It enables the visualization of amyloid accumulation in the brain of AD patients by positron emission tomography (PET) and allows for semiquantitative evaluation of amyloid levels [1]. Previously, we reported that among patients diagnosed with AD by neuropsychological testing or ordinary diagnostic imaging [e.g. magnetic resonance imaging (MRI)], about 20% were rated PiB negative by PiB-PET. These patients are described as having PiB-negative de-

KARGER
Fax +41 61 306 12 34
E-Mail karger@karger.ch
www.karger.com

1420–8008/12/0342–0112$38.00/0

Accessible online at:
www.karger.com/dem

Hiroyuki Shimada, MD
Department of Geriatrics and Neurology
Osaka City University Graduate School of Medicine
1-4-3 Asahimachi, Abeno-ku
Osaka 545-8585 (Japan)
Tel. +81 66 645 3889, E-Mail h.shimada@med.osaka-cu.ac.jp

mentia, and they differ markedly from PiB-positive AD patients in terms of the levels of cerebrospinal fluid (CSF) biomarkers [2]. According to the previous study, PiB-negative dementia is characterized by (1) significantly lower amyloid accumulation in the cortex compared to cases with PiB-positive AD; (2) lack of apolipoprotein E (ApoE) ε4; (3) less marked reduction of $A\beta_{1-42}$ levels in the CSF, and (4) elevation of p-tau levels in the CSF compared to cases of PiB-positive AD.

It is possible that PiB-negative dementia involves not only dementia with Lewy bodies (DLB) and frontotemporal lobar degeneration (FTLD) but also diseases of tauopathy, such as argyrophilic grain disease (AGD) and neurofibrillary tangle-predominant dementia (NFTD). According to recent reports, 2 AD cases that were rated as PiB-negative by PiB-PET showed different primary findings – in one diffuse plaques were the primary pathological feature [3] and in the other PiB-negative Aβ accumulation was the primary finding [4]. In addition, it has been reported that PiB-PET revealed no amyloid accumulation in the cerebral cortex in cases of familial AD [5]. DLB is the second most common cause of dementia after AD in neurodegenerative disorders [6]; hence, DLB seems to be important in the differential diagnosis of PiB-negative dementia.

Yoshita et al. [7] reported that ^{123}I-metaiodobenzylguanidine (MIBG) myocardial scintigraphy provides a sensitive means to distinguish DLB from AD in patients who do not show parkinsonian symptoms. ^{123}I-MIBG myocardial scintigraphy is useful in the differential diagnosis of PiB-negative dementia, particularly for its distinction from DLB. Furthermore, Adachi et al. [8] reported that unilateral atrophy of the anterior part of the hippocampus or ambient gyrus, determined by MRI, is useful in the differential diagnosis of AGD. Voxel-based morphometry (VBM) is used for the analysis of volumetric differences among brain regions [9]. As VBM enables semiquantitative evaluations, it can be used to characterize brain atrophy in the PiB-negative dementia group.

The present study was performed to evaluate cases of PiB-negative dementia by using a variety of methods, including fluorodeoxyglucose (FDG)-PET.

Patients and Methods

Participants

All participants in this study were recruited from patients visiting the outpatient geriatrics and neurology clinic of the Osaka City University Hospital. This clinical study was approved by the Ethics Committee of the Osaka City University School of Medicine, and written informed consent was obtained from all subjects and controls, or from their next of kin in cases with advanced dementia. PiB-PET was performed on 64 patients who were clinically diagnosed with AD in accordance with the NINCDS-ADRDA (National Institute of Neurological and Communicative Disorders and Stroke and the AD and Related Disorders Association) criteria [10] and who provided consent to PiB-PET. PiB-PET findings were assessed in accordance with the criteria reported previously [2], and 14 cases (21.9%) were rated as PiB negative. Of these cases, 11 (4 men and 7 women) consented to undergo the CSF test, VBM, FDG-PET, ^{123}I-MIBG myocardial scintigraphy and genetic screening (*ApoE* gene). These 11 patients were enrolled in this study and were described as cases of PiB-negative dementia. They had a mean age ± SD of 75.7 ± 6.9 years (range, 59–89), a mini-mental state examination (MMSE) score of 22.7 ± 3.1 out of 30 (range, 17–28) and a Rivermead Behavioral Memory Test score of 6.5 ± 4.0 out of 24 (range, 0–16). None of these patients carried the *ApoE* ε4 gene (table 1).

Healthy elderly individuals with normal cognitive function were recruited as controls for each test. We included 8 patients diagnosed with DLB in accordance with the criteria of the third report of the DLB Consortium [11] [7 men and 1 woman; mean age ± SD, 76.1 ± 3.1 years (range, 68–78), and MMSE score, 20.6 ± 3.6 out of 30 (range, 16–26)]; 10 patients with PiB-positive AD [5 men and 5 women; mean age ± SD, 70.2 ± 5.3 years (range, 63–82), and MMSE score, 22.0 ± 2.9 out of 30 (range, 16–26)], and 20 healthy elderly individuals who served as the control group [10 men and 10 women; mean age ± SD, 71.5 ± 6.1 years (range, 61–89), and MMSE score, 28.8 ± 1.6 out of 30 (range, 25–30)].

CSF Biomarkers

CSF samples were obtained from the L3/L4 or L4/L5 interspaces in the morning and collected in 10-ml polypropylene tubes. The samples were aliquoted into 0.5- or 1-ml polypropylene tubes and stored at −80°C until further analysis. We measured the CSF levels of $A\beta_{1-42}$ with an enzyme-linked immunosorbent assay (ELISA) kit (Wako Pure Chemical Industries, Osaka, Japan) and p-tau 181 with a sandwich ELISA kit (Innotest; Innogenetics, Gent, Belgium).

FDG-PET

PET images were obtained with an Eminence-B PET scanner (Shimadzu, Kyoto, Japan). A transmission scan was obtained using a ^{137}Cs pin source for attenuation correction. Emission scans were acquired in the three-dimensional mode with a total axial field of view of 208 mm. PET studies were performed with the subjects in resting condition with eyes closed and ears unplugged while comfortably lying in a darkened and quiet room. All subjects fasted for at least 4 h before PET scanning. After the transmission scan, a 10-min emission scan was performed 50 min after an intravenous injection of 100–120 MBq of FDG. Images were reconstructed by the dynamic row-action maximum-likelihood algorithm (DRAMA), which is a block-iterative algorithm (iteration 1; filter cycle, 128; scatter correction, hybrid dual energy window). The dimensions of the reconstructed PET images were 128 × 128 matrices. PET

Table 1. Characteristics of the PiB-negative dementia patients

Case no.	Age years	Sex	MMSE score	RBMT score	ApoE genotype	PiB MCDVR
1	79	M	24	10	ε3/ε3	1.14
2	78	F	21	4	ε3/ε3	0.98
3	76	F	17	3	ε3/ε3	0.95
4	71	F	23	5	ε3/ε3	0.90
5	76	F	23	0	ε3/ε3	1.08
6	59	F	22	6	ε3/ε3	0.87
7	89	M	21	9	ε2/ε3	0.90
8	77	F	23	5	ε3/ε3	1.00
9	76	F	26	8	ε3/ε3	1.23
10	73	M	26	5	ε3/ε3	0.90
11	79	M	28	16	ε3/ε3	1.23
Mean ± SD	75.7±6.9	4M, 7F	22.7±3.1	6.5±4.0		1.00±0.1

M = male; F = female; MCDVR = mean cortical distribution volume ratio of PiB-PET, cutoff level <1.3; RBMT = Rivermead Behavioral Memory Test (maximum score = 24). Scores are displayed as standardized profile scores. MMSE: maximum score = 30.

image analysis was performed by three-dimensional stereotactic surface projection [12].

^{123}I-MIBG Myocardial Scintigraphy

About 111 MBq of ^{123}I-MIBG (Fujifilm RI Pharma, Tokyo, Japan) were injected intravenously. Planar images of the anterior view of the chest were obtained twice for a duration of 5 min, first 15 min (early phase) and then 180 min (delayed phase) after the injection of ^{123}I-MIBG. Planar scans were performed with a double-head γ-camera (Bright view X with XCT, Philips Healthcare, Best, The Netherlands) that was equipped with low-energy, high-resolution collimators. Relative organ uptake of ^{123}I-MIBG was determined by a region-of-interest analysis in the anterior view. The ratio of the average pixel count in the heart to that in the mediastinum (H/M ratio) was calculated after the early and the delayed phase. Data are expressed as means ± SEM. Statistical differences were determined by two-sided Student's t tests. Differences with values of $p < 0.05$ were considered significant.

MRI

All MR images were obtained with a 1.5-tesla Siemens Avanto MRI scanner (Siemens Medical Solutions, Erlangen, Germany). A T_1-weighted magnetization-prepared rapid gradient echo sequence was used to generate 104 continuous 1.5-mm-thick axial slices [repetition time = 7.0 ms; echo time = 2.66 ms; flip angle = 10°; field of view = 240 mm, and matrix size = 256 × 256).

VBM Analysis

VBM analyses were performed with SPM5 (Wellcome Trust Center for Neuroimaging, London, UK) running on Matlab 7.7.1 (MathWorks, Natick, Mass., USA). MR images were segmented, normalized and modulated with the unified segmentation model. Spatially normalized and modulated gray matter images were then smoothed with a 12-mm full-width half-maximum isotropic Gaussian kernel. Gray matter differences between groups (PiB-negative dementia patients vs. controls and PiB-positive AD patients vs. controls) were assessed with 2-sample t tests within the general linear model framework of SPM. Age, gender, disease severity (determined using the MMSE) and total intracranial volume were entered into the design matrix as nuisance variables. The threshold of group analyses was set at $p < 0.05$ with a correction for multiple comparisons at the cluster level of the entire brain. The intensity threshold applied to the cluster level statistics was set at $p < 0.001$, and the extent threshold in terms of the number of voxels was >10.

Results

^{123}I-MIBG Myocardial Scintigraphy

Figure 1 shows the distribution of the H/M ratios in the early and delayed phases in individual subjects. In the early phase, the mean ± SEM of the H/M ratio was higher in the PiB-negative dementia group (2.08 ± 0.16) than in the healthy control group (1.88 ± 0.17; $p < 0.02$), and the ratio in the PiB-negative dementia group differed markedly from that in the DLB group (1.28 ± 0.11; $p < 0.001$; fig. 1a). In the delayed phase, there was no significant difference in the H/M ratios between the PiB-negative dementia group (2.08 ± 0.19) and the healthy control group (1.94 ± 0.22), but the ratio in the PiB-negative demen-

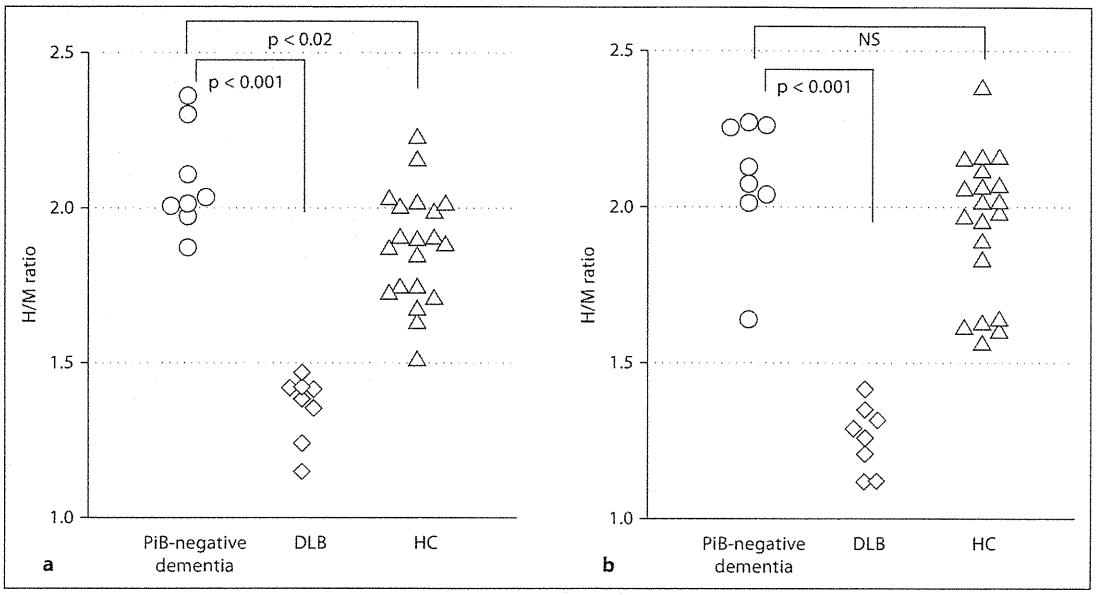

Fig. 1. Comparison of the H/M ratios among healthy controls (HC) and disease groups. For both the early (**a**) and delayed H/M ratios (**b**), patients with PiB-negative dementia (○) showed a significantly higher distribution compared with DLB patients (◇). The H/M ratio of the early phase in healthy controls (△) was significantly lower than that of PiB-negative patients, but no difference was found in the delayed phase. NS = Nonsignificant.

tia group was significantly higher than that in the DLB group (1.28 ± 0.11; $p < 0.001$). Thus, the delayed phase revealed marked differences between the PiB-negative dementia group and the DLB group (fig. 1b).

CSF Biomarkers, MRI and FDG-PET

Table 2 summarizes the CSF biomarker data and the imaging findings. Several characteristic findings are shown in figure 2. In the analysis of the CSF data, cases 8 and 9 showed reductions in $A\beta_{1-42}$ levels and elevations in p-tau levels, and case 5 showed a reduction in $A\beta_{1-42}$ alone. The levels of all CSF biomarkers were within the normal ranges in the other cases. Cases 1–3 showed atrophy of the hippocampus predominantly on the left side (fig. 2a), cases 4 and 5 of both frontal lobes (fig. 2c), case 6 of both temporal lobes, case 7 of both hippocampi and also enlargement of the inferior horn of the lateral ventricle (fig. 2e), and case 9 showed atrophy of both hippocampi. In the other 3 cases, atrophy was not evident. FDG-PET revealed reduced glucose metabolism in the medial temporal lobe in case 3 (fig. 2b), in both frontal lobes in cases 4 and 5 (fig. 2d), and in both temporal lobes in case 6. In the other cases, reductions in glucose metabolism were primarily seen in the parietotemporal lobe and in the cingulate gyrus.

VBM

Figure 3 shows the results of statistical analyses of the location and severity of brain atrophy rated by VBM in the PiB-negative dementia group and the PiB-positive AD group in comparison to the healthy control group. There were no significant differences in age, MMSE scores and education between both groups.

The PiB-negative dementia group showed significant atrophy of the left precuneus compared to the healthy control group ($p < 0.02$). The PiB-positive AD group showed significant atrophy of both the left ($p < 0.001$) and right hippocampus ($p < 0.01$) compared to the healthy control group. No significant associations were noted between MMSE scores and the locations of atrophy.

Discussion

Cases of clinically diagnosed AD that were rated as PiB-negative by amyloid imaging have been reported previously. These cases exhibit characteristic CSF profiles, thereby suggesting that non-AD cases may be present in PiB-negative dementia [2]. We discussed in our previous report that the pathology of these cases probably involves not only DLB and FTLD but also tauopathy

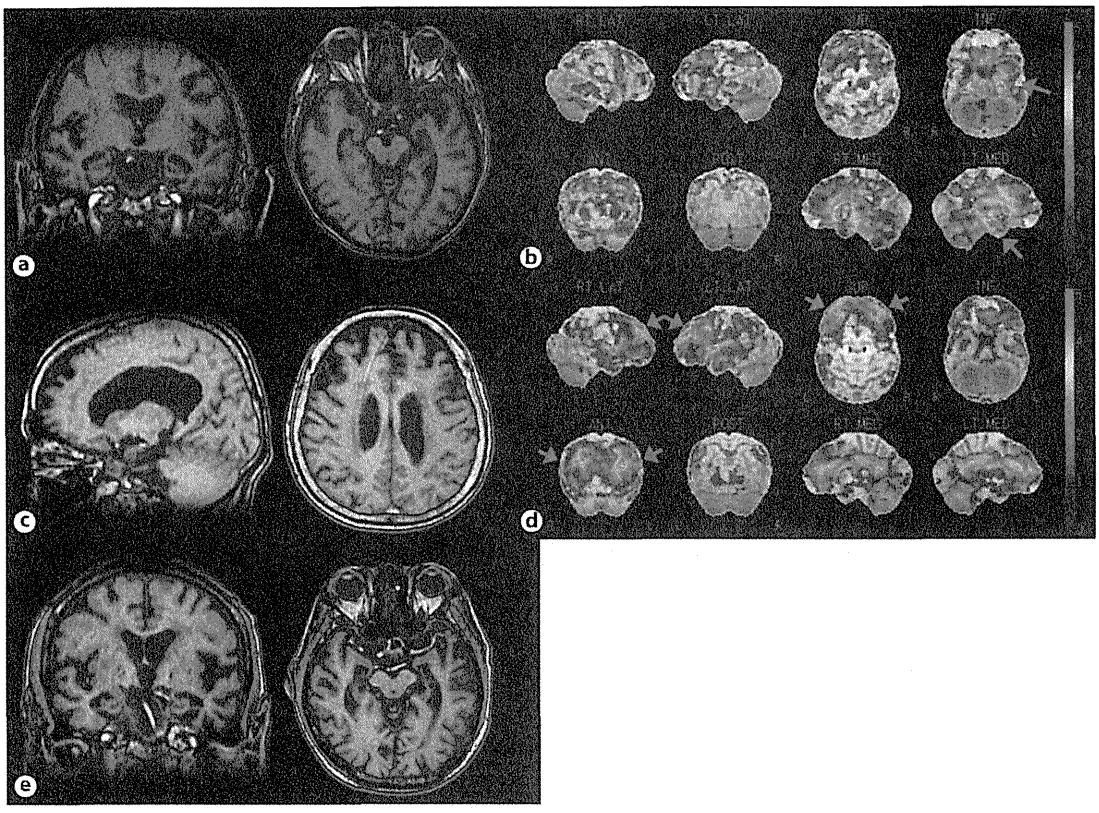

Color version available online

Fig. 2. Imaging findings in individual cases of PiB-negative dementia. **a** In MRI scans (case 1), there is a dilatation of the temporal groove and inferior horn of the lateral ventricle and atrophy of the temporal pole and anterior medial temporal lobe, all with left-sided dominance. **b** An FDG- PET image (case 3) showing hypometabolism of the medial temporal lobe with left-sided dominance (arrow). **c** MR images (case 5) showing marked atrophy of both frontal lobes. **d** FDG-PET images of the same case showing hypometabolism of both frontal lobes (arrow). **e** MR images (case 7) showing atrophy of both hippocampi with enlarged inferior horns of the lateral ventricles.

(e.g. AGD and NFTD) and even AD itself. The present study was performed to investigate the pathology of PiB-negative dementia by using various neuroradiological tests.

In the analysis with ^{123}I-MIBG myocardial scintigraphy, the H/M ratio in the early phase did not markedly differ between the PiB-negative dementia group and the healthy control group, although it was slightly higher in the former group. The ratio in the PiB-negative dementia cases was significantly higher than that in the DLB group ($p < 0.001$; fig. 1). It has been reported that PiB-PET showed a diffuse increase in amyloid accumulation in the cerebral cortex in about 60–80% of all DLB cases, and this finding has been confirmed in autopsy cases [13, 14]. Conversely, other DLB patients with poor amyloid deposition have been reported to be PiB negative. Because these patients were relatively younger (<65 years old), these findings were not consistent with those noted in the cases with PiB-negative dementia who were enrolled in this study (table 1). The sensitivity and specificity of ^{123}I-MIBG uptake as an indicator for the distinction of DLB and Parkinson's disease among demented patients were reported to be 98 and 94%, respectively, by Treglia and Cason [15] and 95 and 87%, respectively, by Hanyu et al. [16]. MIBG scintigraphy provides a valuable means for the differential diagnosis of DLB from other dementias. Our results of ^{123}I-MIBG myocardial scintigraphy showed marked differences between the DLB group and the healthy control group and between the DLB group and the PiB-negative dementia group. These findings suggest that it is unlikely that DLB is involved in the pathology of the PiB-negative dementia.

Table 2. Imaging findings of PiB-negative dementia patients and CSF levels of biomarkers

Case no.	CSF $A\beta_{1-42}$ pg/ml	CSF p-tau pg/ml	MIBG H/M ratio		MRI atrophy region	FDG-PET decreased region
			early	delayed		
1	738	40.8	1.87	1.64	bil. hippocampus (LT > RT)	LT parietotemporal, LT post.cingulate-precuneus
2	545	42.8	2.30	2.27	bil. hippocampus (LT > RT)	LT frontotemporal, bil. cingulate
3	936	76.9	1.98	2.01	bil. hippocampus (LT > RT)	bil. cingulate; bil. medial temporal (LT > RT)
4	1,031	66.4	NE	NE	bil. frontal	bil. frontal, bil. cingulate
5	254	31.4	NE	NE	bil. frontal	bil. frontal, bil. cingulate
6	1,107	31.1	2.01	2.25	bil. temporal	bil. temporal
7	594	55.4	NE	NE	bil. hippocampus	bil. parietotemporal
8	405	161	2.11	2.26	(–)	bil. parietotemporal, bil. frontal
9	452	144	2.02	2.04	bil. hippocampus	RT parietotemporal, RT frontal, bil. cingulate
10	484	27.9	2.36	2.07	(–)	bil. cingulate, bil.temporal
11	815	71.7	2.04	2.13	(–)	bil. parietotemporal (LT > RT)
Mean ± SD	669.2±263.6	68.1±43.0	2.08±0.15	2.08±0.19		

CSF biomarker: increase in CSF p-tau and decreased CSF $A\beta_{1-42}$ (cases 8 and 9); MRI: hippocampal atrophy with left-sided dominance (cases 1–3), frontal lobe atrophy on both sides (cases 4 and 5) and temporal lobe atrophy on both sides (case 6); FDG-PET: hypometabolism of the medial temporal lobe with left-sided dominance (case 3), hypometabolism of both frontal lobes (cases 4 and 5), and hypometabolism of both temporal lobes (case 6). bil. = Bilateral; LT = left; RT = right; NE = not examined; post. = posterior. Normal: CSF $A\beta_{1-42}$ >450 pg/ml and CSF p-tau <75 pg/ml.

MRI and FDG-PET revealed unilateral atrophy of the hippocampus as well as reduced glucose metabolism in the unilateral medial temporal lobe (table 2; cases 1–3), which is consistent with the characteristic features of AGD proposed by Adachi et al. [8]. Furthermore, cases 4–6 are supposed to have FTLD because these cases showed atrophy of both frontal or temporal lobes by MRI and reduced glucose metabolism in the same region by FDG-PET. As far as the features shown on MRI and FDG-PET of AGD and FTLD are concerned, differential diagnosis will be impossible to some extent during routine clinical practice without these radiological tests.

According to the guidelines for clinical diagnosis proposed by Yamada [17], the diagnosis of 1 case was consistent with NFTD (case 7). As there have been no reported functional imaging studies of pathologically confirmed NFTD cases, it seems difficult to use such techniques for the distinction of NFTD from AD. Furthermore, in our previous report [2], the CSF biomarkers in these 7 cases (cases 1–7) did not follow the typical pattern that is known for AD (reduction of $A\beta_{1-42}$ levels and elevation of p-tau levels in the CSF; table 2). These results suggest that cases of clinically suspected AD are likely to include cases having diseases of tauopathy, such as FTLD, AGD and NFTD. Because cases diagnosed with a combination of conditions (AD + AGD) have been reported [18], those presenting with atypical courses need to be evaluated with more detailed psychological tests and diagnostic examinations other than amyloid imaging.

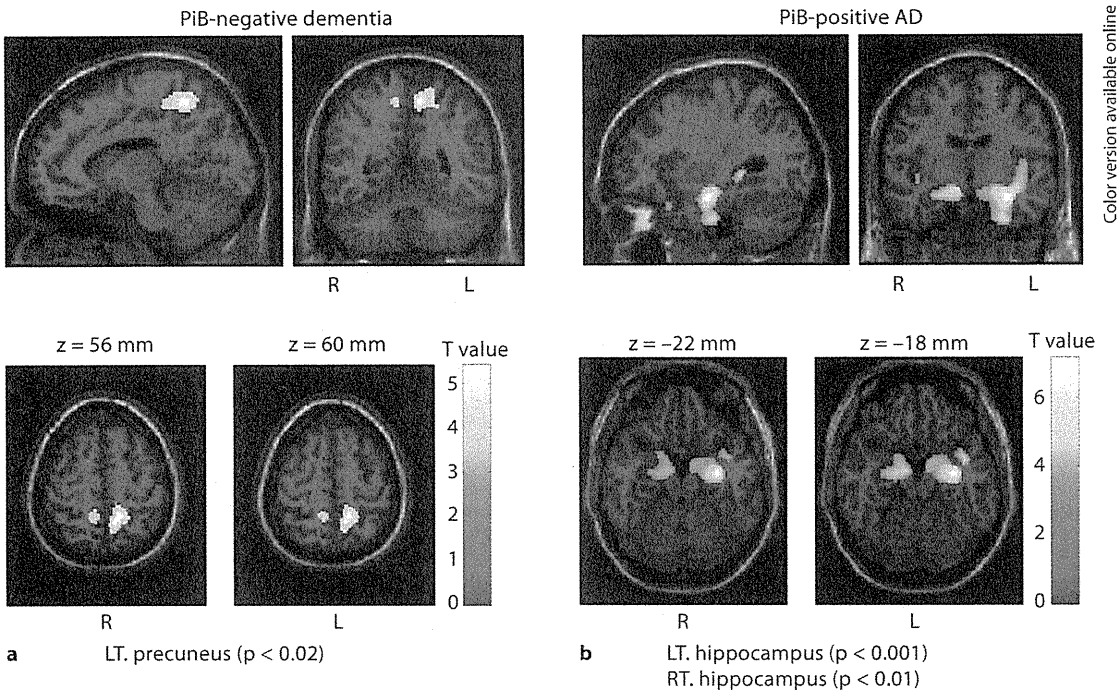

Fig. 3. Statistical parametric maps comparing the gray matter volume of patients with that of healthy controls. **a** The PiB-negative dementia patient group was compared with the healthy control group, and significant atrophy was found in the left precuneus ($p < 0.02$). **b** Comparisons of the PiB-positive AD group and the healthy control group showed significant atrophy in the left ($p < 0.001$) and right hippocampus ($p < 0.01$). The color bar values indicate the value of the T statistic in each display.

In addition, there were 2 cases who had test results consistent with AD (reduction of $A\beta_{1-42}$ levels, elevation of p-tau levels in the CSF and reduced glucose metabolism in the parietotemporal lobe) determined by FDG-PET (cases 8 and 9). PiB-negative AD cases with primary pathological findings of diffuse plaques [3] or Aβ proteins that bind less PiB [4] have been reported, supporting the necessity for additional pathological evaluations of PiB-negative cases.

For quantitative evaluation of brain atrophy, we used VBM in the present study and found marked atrophy in both hippocampi in the AD group, which is consistent with a previous report [19], and marked atrophy of the precuneus in the PiB-negative dementia group (fig. 3). According to a recent report, functional MRI findings suggest that the precuneus forms part of the default mode network at rest and that there is a close association between the default mode network and episodic memories [20]. Furthermore, patients with AD tend to show interruption of the default mode network compared to healthy elderly controls, and Sheline et al. [21] reported that amyloid deposition is involved in this interruption. However, because the PiB-negative dementia group was apparently free of amyloid deposition, the identification of other factors involved in the interruption of the default mode network is needed. Recent studies have demonstrated that precuneus atrophy is a characteristic of early-onset AD [22, 23]. However, this finding was not supported in the present study because the PiB-negative dementia group did not include young patients. Therefore, it seems likely that, as described above, the PiB-negative dementia group presents disturbances in the default mode network through pathophysiological mechanisms that differ from AD, as shown by the differences observed in the CSF biomarkers and findings from diagnostic imaging. This disturbance in the default network of PiB-negative dementia patients results in a primarily episodic memory disorder that is clinically akin to AD. Analysis of the VBM data from all cases with PiB-negative dementia did not reveal unilateral atrophy

of the anterior part of the hippocampus or ambient gyrus that is characteristic of AGD. This is not surprising as the PiB-negative dementia group is not composed of patients with a single disease such as AGD.

The limitations of the present study are that the limited number of cases studied and the short follow-up period which did not facilitate longitudinal observations. In a larger patient cohort with a longer follow-up, it might be possible to further elucidate the pathological features of cases with PiB-negative dementia.

These results suggest that PiB-negative dementia cases are conventionally diagnosed as AD in medical facilities. However, PiB-negative dementia cases are not good candidates for anti-amyloid treatment, such as bapineuzumab. The understanding of the differences in the pathological features of AD and PiB-negative dementia will further improve the accuracy of the clinical diagnosis of AD. To date, postmortem pathological examinations of PiB-negative dementia cases have not been reported. However, all the PiB-negative dementia cases in this study are being followed up at our facility, and autopsies of these cases in the future will reveal the pathological features of PiB-negative dementia in greater detail.

References

1 Klunk WE, Engler H, Nordberg A, Wang Y, Blomqvist G, Holt DP, Bergstrom M, Savitcheva I, Huang GF, Estrada S, Ausen B, Debnath ML, Barletta J, Price JC, Sandell J, Lopresti BJ, Wall A, Koivisto P, Antoni G, Mathis CA, Langstrom B: Imaging brain amyloid in Alzheimer's disease with Pittsburgh compound-B. Ann Neurol 2004;55:306–319.

2 Shimada H, Ataka S, Takeuchi J, Mori H, Wada Y, Watanabe Y, Miki T: Pittsburgh compound B-negative dementia – a possibility of misdiagnosis of patients with non-Alzheimer disease-type dementia as having AD. J Geriatr Psychiatry Neurol 2011;24:123–126.

3 Cairns NJ, Ikonomovic MD, Benzinger T, Storandt M, Fagan AM, Shah AR, Reinwald LT, Carter D, Felton A, Holtzman DM, Mintun MA, Klunk WE, Morris JC: Absence of Pittsburgh compound B detection of cerebral amyloid beta in a patient with clinical, cognitive, and cerebrospinal fluid markers of Alzheimer disease: a case report. Arch Neurol 2009;66:1557–1562.

4 Rosen RF, Ciliax BJ, Wingo TS, Gearing M, Dooyema J, Lah JJ, Ghiso JA, LeVine H, Walker LC: Deficient high-affinity binding of Pittsburgh compound B in a case of Alzheimer's disease. Acta Neuropathol 2009;119:221–233.

5 Shimada H, Ataka S, Tomiyama T, Takechi H, Mori H, Miki T: Clinical course of patients with familial early-onset Alzheimer's disease potentially lacking senile plaques bearing the E693Delta mutation in amyloid precursor protein. Dement Geriatr Cogn Disord 2011;32:45–54.

6 Kosaka K: Diffuse Lewy body disease. Neuropathology 2000;20(suppl):S73–S78.

7 Yoshita M, Taki J, Yokoyama K, Noguchi-Shinohara M, Matsumoto Y, Nakajima K, Yamada M: Value of ^{123}I-MIBG radioactivity in the differential diagnosis of DLB from AD. Neurology 2006;66:1850–1854.

8 Adachi T, Saito Y, Hatsuta H, Funabe S, Tokumaru AM, Ishii K, Arai T, Sawabe M, Kanemaru K, Miyashita A, Kuwano R, Nakashima K, Murayama S: Neuropathological asymmetry in argyrophilic grain disease. J Neuropathol Exp Neurol 2010;69:737–744.

9 Ashburner J, Friston KJ: Voxel-based morphometry – the methods. Neuroimage 2000;11:805–821.

10 McKhann G, Drachman D, Folstein M, Katzman R, Price D, Stadlan EM: Clinical diagnosis of Alzheimer's disease: report of the NINCDS-ADRDA Work Group under the auspices of Department of Health and Human Services Task Force on Alzheimer's Disease. Neurology 1984;34:939–944.

11 McKeith IG, Dickson DW, Lowe J, Emre M, O'Brien JT, Feldman H, Cummings J, Duda JE, Lippa C, Perry EK, Aarsland D, Arai H, Ballard CG, Boeve B, Burn DJ, Costa D, Del Ser T, Dubois B, Galasko D, Gauthier S, Goetz CG, Gomez-Tortosa E, Halliday G, Hansen LA, Hardy J, Iwatsubo T, Kalaria RN, Kaufer D, Kenny RA, Korczyn A, Kosaka K, Lee VM, Lees A, Litvan I, Londos E, Lopez OL, Minoshima S, Mizuno Y, Molina JA, Mukaetova-Ladinska EB, Pasquier F, Perry RH, Schulz JB, Trojanowski JQ, Yamada M: Diagnosis and management of dementia with Lewy bodies: third report of the DLB Consortium. Neurology 2005;65:1863–1872.

12 Minoshima S, Frey KA, Koeppe RA, Foster NL, Kuhl DE: A diagnostic approach in Alzheimer's disease using three-dimensional stereotactic surface projections of fluorine-18-FDG PET. J Nucl Med 1995;36:1238–1248.

13 Gomperts SN, Rentz DM, Moran E, Becker JA, Locascio JJ, Klunk WE, Mathis CA, Elmaleh DR, Shoup T, Fischman AJ, Hyman BT, Growdon JH, Johnson KA: Imaging amyloid deposition in Lewy body diseases. Neurology 2008;71:903–910.

14 Foster ER, Campbell MC, Burack MA, Hartlein J, Flores HP, Cairns NJ, Hershey T, Perlmutter JS: Amyloid imaging of Lewy body-associated disorders. Mov Disord 2010;25:2516–2523.

15 Treglia G, Cason E: Diagnostic performance of myocardial innervation imaging using MIBG scintigraphy in differential diagnosis between dementia with Lewy bodies and other dementias: a systematic review and a meta-analysis. J Neuroimaging 2012;22:111–117.

16 Hanyu H, Shimizu S, Hirao K, Sakurai H, Iwamoto T, Chikamori T, Hida S, Yamashina A, Koizumi K, Abe K: The role of ^{123}I-metaiodobenzylguanidine myocardial scintigraphy in the diagnosis of Lewy body disease in patients with dementia in a memory clinic. Dement Geriatr Cogn Disord 2006;22:379–384.

17 Yamada M: Senile dementia of the neurofibrillary tangle type (tangle-only dementia): neuropathological criteria and clinical guidelines for diagnosis. Neuropathology 2003;23:311–317.

18 Saito Y, Murayama S: Neuropathology of mild cognitive impairment. Neuropathology 2007;27:578–584.
19 Rombouts SA, Barkhof F, Witter MP, Scheltens P: Unbiased whole-brain analysis of gray matter loss in Alzheimer's disease. Neurosci Lett 2000;285:231–233.
20 Greicius MD, Srivastava G, Reiss AL, Menon V: Default-mode network activity distinguishes Alzheimer's disease from healthy aging: evidence from functional MRI. Proc Natl Acad Sci USA 2004;101:4637–4642.
21 Sheline YI, Raichle ME, Snyder AZ, Morris JC, Head D, Wang S, Mintun MA: Amyloid plaques disrupt resting state default mode network connectivity in cognitively normal elderly. Biol Psychiatry 2010;67:584–587.
22 Karas G, Scheltens P, Rombouts S, Schijndel R, Klein M, Jones B, Flier W, Vrenken H, Barkhof F: Precuneus atrophy in early-onset Alzheimer's disease: a morphometric structural MRI study. Neuroradiology 2007;49:967–976.
23 Shiino A, Watanabe T, Kitagawa T, Kotani E, Takahashi J, Morikawa S, Akiguchi I: Different atrophic patterns in early- and late-onset Alzheimer's disease and evaluation of clinical utility of a method of regional z-score analysis using voxel-based morphometry. Dement Geriatr Cogn Disord 2008;26:175–186.

RESEARCH ARTICLE

β-Amyloid in Lewy Body Disease is Related to Alzheimer's Disease-Like Atrophy

Hitoshi Shimada, MD, PhD,[1,2] Hitoshi Shinotoh, MD, PhD,[1,3] Shigeki Hirano, MD, PhD,[1,4] Michie Miyoshi, MD, PhD,[1] Koichi Sato, MD, PhD,[1,5] Noriko Tanaka, MD, PhD,[1] Tsuneyoshi Ota, MD, PhD,[1,6] Kiyoshi Fukushi, PhD,[7] Toshiaki Irie, PhD,[7] Hiroshi Ito, MD, PhD,[8] Makoto Higuchi, MD, PhD,[1] Satoshi Kuwabara, MD, PhD,[4] and Tetsuya Suhara, MD, PhD[1]*

[1]*Molecular Imaging Center, Molecular Neuroimaging Program, National Institute of Radiological Sciences, Chiba, Japan*
[2]*Section for Human Neurophysiology, Research Center for Frontier Medical Engineering, Chiba University, Chiba, Japan*
[3]*Neurology Chiba, Chiba, Japan*
[4]*Department of Neurology, Graduate School of Medicine, Chiba University, Chiba, Japan*
[5]*Department of Psychiatry, Teikyo University Chiba Medical Center, Chiba, Japan*
[6]*Department of Psychiatry, Juntendo University School of Medicine, Tokyo, Japan*
[7]*Molecular Imaging Center, Molecular Probe Program, National Institute of Radiological Sciences, Chiba, Japan*
[8]*Molecular Imaging Center, Biophysics Program, National Institute of Radiological Sciences, Chiba, Japan*

ABSTRACT: The aim of this study was to investigate whether amyloid deposition is associated with Alzheimer's disease (AD)-like cortical atrophy in Lewy body (LB) disease (LBD). Participants included 15 LBD with dementia patients (8 with dementia with Lewy bodies [DLB] and 7 with Parkinson's disease [PD] with dementia [PDD]), 13 AD patients, and 17 healthy controls. Age, gender, and Mini–Mental State Examination scores were matched between patient groups. All subjects underwent PET scans with [^{11}C]Pittsburgh Compound B to measure brain amyloid deposition as well as three-dimensional T1-weighted MRI. Gray-matter volumes (GMVs) were estimated by voxel-based morphometry. Volumes-of-interest analyses were also performed. Forty percent of the 15 DLB/PDD patients were amyloid positive, whereas all AD patients and none of the healthy controls were amyloid positive. Amyloid-positive DLB/PDD and AD patients showed very similar patterns of cortical atrophy in the parahippocampal area and lateral temporal and parietal cortices, with 95.2% of cortical atrophy distribution being overlapped. In contrast, amyloid-negative DLB/PDD patients had no significant cortical atrophy. Compared to healthy controls, parahippocampal GMVs were reduced by 26% in both the amyloid-positive DLB/PDD and AD groups and by 10% in the amyloid-negative DLB/PDD group. The results suggest that amyloid deposition is associated with AD-like atrophy in DLB/PDD patients. Early intervention against amyloid may prevent or delay AD-like atrophy in DLB/PDD patients with amyloid deposition.

Key Words: voxel-based morphometry; dementia with Lewy bodies; Parkinson's disease with dementia; Alzheimer's disease; amyloid PET

Dementia with Lewy bodies (DLB) and Parkinson's disease (PD) with dementia (PDD) are categorized as belonging to the same spectrum: LBD with dementia.[1] In addition to pathognomonic Lewy body (LB) pathology, DLB/PDD patients frequently have Alzheimer's disease (AD)-type pathology, particularly amyloid beta (Aβ) plaque.[2] The contribution of Aβ to the development of DLB/PDD remains unclear.

[^{11}C]Pittsburgh compound B (PIB) is a well-established compound for amyloid imaging with PET.[3] An *in vitro* binding study indicated that the PIB retention observed in DLB is largely attributable to PIB binding to Aβ plaque, but not to LBs.[4] More than half of DLB patients and approximately one third of PDD patients had cortical Aβ burden in previous studies using

Additional Supporting Information may be found in the online version of this article.

***Correspondence to:** Dr. Tetsuya Suhara, Molecular Neuroimaging Program, Molecular Imaging Center, National Institute of Radiological Sciences, 4-9-1 Anagawa, Inage-ku, Chiba-shi, Chiba, 263-8555, Japan; suhara@nirs.go.jp

Funding agencies: A part of this work was supported by the Japan Advanced Molecular Imaging Program of the Ministry of Education, Culture, Sports, Science, and Technology, Japan, a Grant-in-Aid for Scientific Research on Innovative Areas from the Ministry of Education, Culture, Sports, Science, and Technology, Japan, and a Grant-in-Aid for Comprehensive Research on Dementia (no. 11103404) from the Ministry of Health, Labor, and Welfare.

Relevant conflicts of interest/financial disclosures: Nothing to report. Full financial disclosures and author roles may be found in the online version of this article.

Received: 30 June 2012; **Revised:** 8 October 2012; **Accepted:** 21 October 2012

Published online in Wiley Online Library (wileyonlinelibrary.com).
DOI: 10.1002/mds.25286

[^{11}C]PIB-PET.[5,6] Maetzler et al. reported that apolipoprotein E ε4 allele prevalence was higher and cerebrospinal fluid A $_{42}$ levels were lower in DLB/PDD patients with PIB retention, compared to those without, suggesting that DLB/PDD patients with cortical Aβ deposition show similar characteristics to AD.[5] However, there has been no study on the effect of cortical Aβ load on cortical atrophy in DLB/PDD. Previous MRI volumetric studies suggested that DLB/PDD patients showed cortical atrophy in several brain regions, including the parahippocampal area. Weintraub et al. reported that AD-like cortical atrophy may be a preclinical biomarker of cognitive decline in PD.[7] However, it is still unclear whether or not the AD-like brain atrophy observed in DLB/PDD is associated with Aβ burden.

To elucidate this issue, we compared the gray-matter volume (GMV) measured by voxel-based morphometry (VBM) among DLB/PDD patients with and without cortical Aβ burden, AD patients, and healthy control subjects.

Patients and Methods

Subjects

Participants included 8 patients with DLB, 7 patients with PDD, and 13 patients with late-onset AD. Twenty-two healthy controls (HCs) without a history of neurologic disorders and abnormalities, assessed by physical and neurologic examinations, were recruited. Five of the twenty-two HC subjects (22.7%), who were diagnosed as PIB positive (PIB(+)) by visual assessment of distribution volume ratio (DVR) images of [^{11}C]PIB PET (see the method for creating DVR images), were excluded. Finally, the other 17 PIB-negative (PIB(−)) HC subjects, in whom PIB uptake of any gray-matter lesions were lower than that of white matter, were included for further analyses as the HC group. DLB patients met the criteria of the third report of the DLB Consortium for probable DLB.[8] Diagnosis of PDD was made in patients fulfilling explicit PD criteria[9] who also fulfilled criteria for dementia based on the *Diagnostic and Statistical Manual of Mental Disorders*, 4th edition.[10] PDD and DLB were distinguished according to the 1-year rule between onset of dementia and that of parkinsonism.[8] Diagnosis of AD was based on the National Institute of Neurological and Communicative Disease and Stroke/Alzheimer's Disease and Related Disorders Association criteria.[11]

All patients were assessed using the Mini–Mental State Examination (MMSE)[12] for global cognitive status, frontal assessment battery (FAB)[13] for dysexecutive syndrome, and neuropsychiatry inventory (NPI)[14] for neuropsychiatric symptoms, and parkinsonian symptoms of all DLB and PDD patients were evaluated by the UPDRS motor subscale.[15] The PET study was approved by the institutional review board of the National Institute of Radiological Sciences. Written informed consent was obtained from all subjects or from their spouses or other close family members.

PET Scan

PET images were acquired by a Siemens ECAT EXACT HR+ scanner (CTI PET Systems, Inc., Knoxville, TN) with an axial field of view of 155 mm, providing 63 contiguous 2.46-mm slices with 5.6-mm transaxial and 5.4-mm axial resolution. A 10-minute transmission scan was performed to measure tissue attenuation. Dynamic emission scan data were acquired in three-dimensional (3D) mode for 90 minutes. Subjects were examined with their eyes closed and their ears unplugged in a quiet room, and their heads were restrained with a band extending across the forehead attached to the headrest. An examiner carefully monitored head movement with laser beams during each scan, and corrections to head position were made in case of movement. Before PET scanning, a dose (370 ± 34 MBq in 5mL) of [^{11}C]PIB was intravenously injected for 60 seconds by infusion pump into the right cubital vein. The PET measurement protocol was based on the previously reported method,[16,17] with some modifications. In brief, a sequence of 19 scans was acquired during 90 minutes (3 × 20 seconds, 3 × 40 seconds, 1 × 1 minute, 2 × 3 minutes, 5 × 6 minutes, and 5 × 10 minutes). All data processing and image reconstruction, including scatter correction, were performed using standard Siemens software.

MRI Acquisition

MRIs were obtained on a 1.5-T Intera (Philips Medical Systems, Best, Netherlands) on the same day as the PET study. Subjects were scanned with a 3D T1-weighted turbo-gradient echo sequence (repetition time/echo time range, 16/5.2 msec; field of view, 256 mm; matrix, 256 × 256; 192 contiguous axial slices of 1.0-mm thickness).

PET Data Preprocessing

All imaging data were preprocessed and analyzed with statistical parametric mapping software (*SPM5*; Wellcome Department of Cognitive Neurology, London, UK), operating in the *MATLAB* software environment (version 7.8; MathWorks, Natick, MA). Each T1-weighted MRI scan was coregistered to each PET image, and spatial normalization of MRI images to the SPM5 T1 MRI template was applied to the PET images.

To minimize, including the white-matter component, volumes of interest (VOIs) of individual cerebellar cortices were manually identified on fusion images of MRI and coregistered summed PET images between 0 and 10 minutes, which reflect cerebral blood flow. PET images were smoothed with an isotropic 12-mm full width at half maximum of Gaussian kernel after

normalization. Then, we estimated DVR using Logan plot graphical analysis, with the cerebellum as the reference region. Atrophy correction was not performed. We used custom software designed by IDL (version 6.0; Jicoux Datasystems, Inc., Tokyo, Japan) to calculate a voxel-based DVR from each image. VOIs were identified on DVR images in each subject's frontal, medial, and lateral temporal, parietal, occipital, anterior, and posterior cingulate and sensorimotor cortices and striatum in both hemispheres using the Wake Forest University (WFU) PickAtlas.[18] Mean cortical DVRs were calculated for each subject as the mean of each value for that subject's frontal, temporal, parietal, and occipital cortices in both hemispheres.

Subjects with significantly increased DVR greater than or equal to mean +2.5 standard deviations (SDs) of the HC group in at least one brain region were classified as PIB(+), and subjects with no significantly increased PIB uptake in any brain region were classified as PIB(−). Furthermore, voxel-based analysis of DVR among the HC, PIB(−) PIB(+) DLB/PDD, and AD groups was performed.

VBM

We performed VBM analysis using the unified segmentation approach implemented in *SPM5* for each 3D T1-weighted MRI.[19,20] Total intracranial volume (TIV) was computed using the native-space tissue maps of each subject. First, regions in which GMV was significantly reduced in the PIB(−) and PIB(+) DLB/PDD groups, compared to the HC group, were estimated. Direct comparisons of GMV among the PIB(−) and PIB(+) DLB/PDD and AD groups were also performed. Second, for the purpose of confirming whether the significant voxels observed in the above-mentioned analysis were AD-like or not, we calculated the GMV overlap ratio of regions in which GMV was significantly reduced, compared to the HC group, in the PIB(+) and PIB(−) DLB/PDD groups and which overlapped with those in the AD group.

Furthermore, the correlation between mean cortical DVR and voxel-by-voxel GMV was analyzed in patients with PIB(+) and (−) DLB/PDD.

VOIs were identified on modulated, normalized, and warped class images in bilateral parahippocampal areas, in which AD patients characteristically show the greatest atrophy—frontal, lateral temporal, parietal, occipital and sensorimotor cortices, striatum, hippocampus, and amygdala—in both hemispheres using the WFU PickAtlas. GMVs of each area were normalized by TIV, and, by using the HC group, each of the assessed Z scores of volume reduction was calculated for further comparison among the AD and PIB(+) DLB/PDD and PIB(−) DLB/PDD groups.

Statistical Analysis

Group comparisons in demographic variables were performed by one-way analysis of variance (ANOVA), followed by Bonferroni's correction. VOI analyses were performed by rank analysis of covariance (rank ANCOVA), adjusting for differences in age, followed by Bonferroni's correction. Correlation analysis between mean cortical DVR and each neuropsychological test score was performed in AD and DLB/PDD patients. Correlation analysis between mean cortical DVR and UPDRS motor score (items 18–31) was also performed in all DLB/PDD patients. All statistical analyses were performed using Statistical Package for the Social Sciences software (*SPSS version 19*; SPSS, Inc., Chicago, IL). In the SPM analysis of MRI, false discovery rate [FDR] corrected, $P < 0.05$, extent threshold > 400 was considered significant.

TABLE 1. Demographic and neuropsychological test results of participants

	HC	DLB/PDD	AD
Number of subjects	17	15 (DLB 8/PDD 7)	13
Male/female	11:6	9:6	3:10
Age	68.3 ± 9.7	72.9 ± 5.6	75.7 ± 4.6
Disease duration, years	—	4.8 ± 2.5	3.0 ± 1.9
UPDRS motor part	—	30.6 ± 16.6	—
MMSE	28.2 ± 2.1	21.8 ± 3.2	19.5 ± 2.7
FAB	15.8 ± 1.6	11.5 ± 3.5	11.7 ± 3.6
NPI	0.1 ± 0.5	7.2 ± 6.6	5.3 ± 6.7

Values are listed as mean ± SD.

Results

Patients with AD were older than the HC group ($F(2, 42) = 4.1$, $P = 0.024$; one-way ANOVA). There was no significant difference in gender among the HC, AD, and DLB/PDD groups (Table 1). MMSE scores in the AD and DLB/PDD groups were lower than those in the HC group ($F(2, 42) = 44.8$, $P \leq 0.001$; one-way ANOVA), whereas MMSE scores did not differ between the AD and DLB/PDD groups ($P = 0.074$).

PET

All HCs were PIB(−), and all AD patients were PIB(+). Half (4 of 8) of the DLB patients and 29% (2 of 7) of the PDD patients were PIB(+). There were no significant differences between the PIB(−) and PIB(+) DLB/PDD groups with respect to the ratio of DLB to PDD patients, age, gender, disease duration, any performed psychological tests even in any subscale, and total score or any subscore of the UPDRS motor subscale (Supporting Table 1).

All PIB(+) DLB/PDD patients showed a similar distribution pattern of increased DVR in the brain to AD patients, where the most marked increase of DVR was observed in parietal association and lateral temporal cortices, compared to the HC group (Fig. 1;

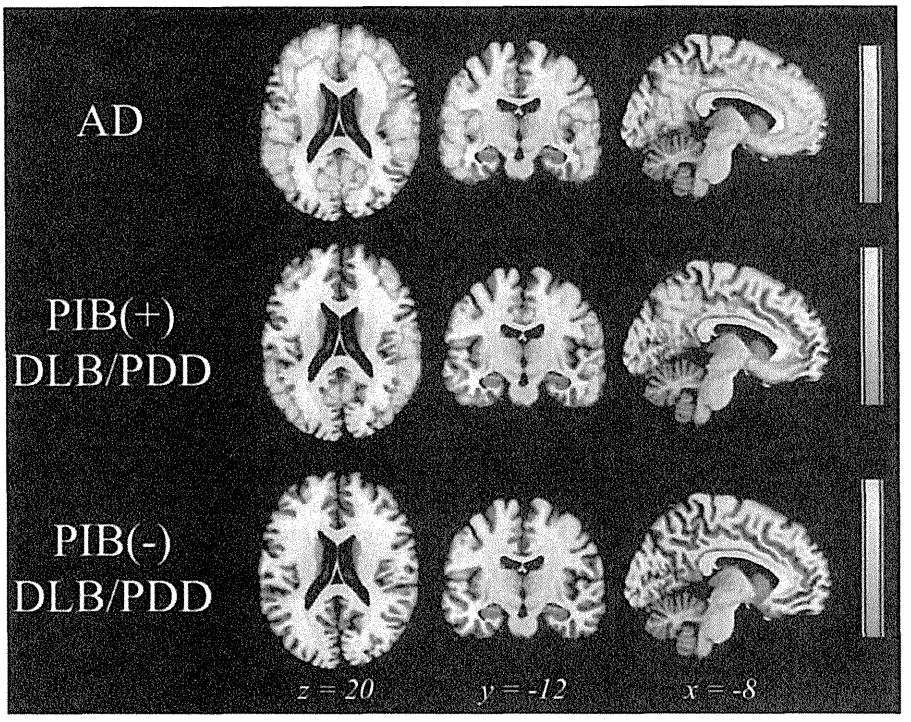

FIG. 1. Statistical parametric map of comparisons between three patient groups and controls in PIB uptake. Regions with significant increase in DVR, an index of amyloid deposition, were observed in AD, PIB(+) DLB/PDD, and PIB(−) DLB/PDD, compared to healthy controls (family-wise error corrected, $P < 0.05$, extent threshold > 200).

Supporting Table 2). The PIB(−) DLB/PDD group had similar DVRs to the HC group in all brain regions.

There were no significant correlations between mean cortical DVR and any neuropsychological test scores and UPDRS motor scores in both the AD and PIB(+) DLB/PDD groups.

VBM

SPM analysis showed more-profound cortical atrophy in both the AD and PIB(+) DLB/PDD groups than in the HC group, especially in the temporal (including the parahippocampus) and parietal areas (including the precuneus) (Fig. 2A), whereas the PIB(−) DLB/PDD group did not show significant cortical atrophy. The AD group showed cortical atrophy, especially in the parietal (including the precuneus), temporal (including the parahippocampus), and frontal cortices, compared to the PIB(−) DLB/PDD group, whereas there was no significant difference in GMV between the AD and PIB(+) DLB/PDD groups or between the PIB(+) and PIB(−) DLB/PDD groups (Supporting Fig. 1). The brain regions in which GMV was significantly reduced, compared to the HC group, in the PIB(+) and PIB(−) DLB/PDD groups overlapped with those in the AD group by 95.2% and 0%, respectively (Fig. 2B).

There was no significant correlation between mean cortical DVR and voxel-by-voxel GMV in PIB(+) and PIB(−) DLB/PDD or in AD patients.

VOI analysis demonstrated a significant difference in parahippocampal GMVs among the HC, AD, PIB(−), and PIB(+) DLB/PDD groups ($F(3,41) = 9.7$, $P < 0.001$, rank ANCOVA; Fig. 3). Bonferroni's post-hoc analysis revealed that, compared to the HC group, parahippocampal GMVs were reduced in both the PIB(+) DLB/PDD (Z-score = 1.94 ± 0.60; $P = 0.002$; 25.8% reduction) and AD (1.91 ± 0.78; $P < 0.001$; 25.5% reduction) groups, whereas those in the PIB(−) DLB/PDD group did not differ from the HC group (0.76 ± 0.60; $P = 1.000$; 10.2% reduction). Compared to PIB(−) DLB/PDD patients, parahippocampal GMVs were reduced in the PIB(+) DLB/PDD ($P = 0.041$) and AD groups ($P = 0.030$). There were no significant differences in parahippocampal GMVs between the AD and PIB(+) DLB/PDD groups ($P = 1.000$). Furthermore, in the AD and PIB(+) DLB/PDD groups, significant GMV reduction, compared to controls, was shown in frontal, parietal, occipital and lateral temporal cortices, striatum, hippocampus, and amygdala, whereas there was no significant GMV reduction in the PIB(−) DLB/PDD group (Table 2).

Discussion

The present study demonstrated that DLB/PDD patients with high cortical PIB uptake had AD-like cortical atrophy in the parahippocampal area as well

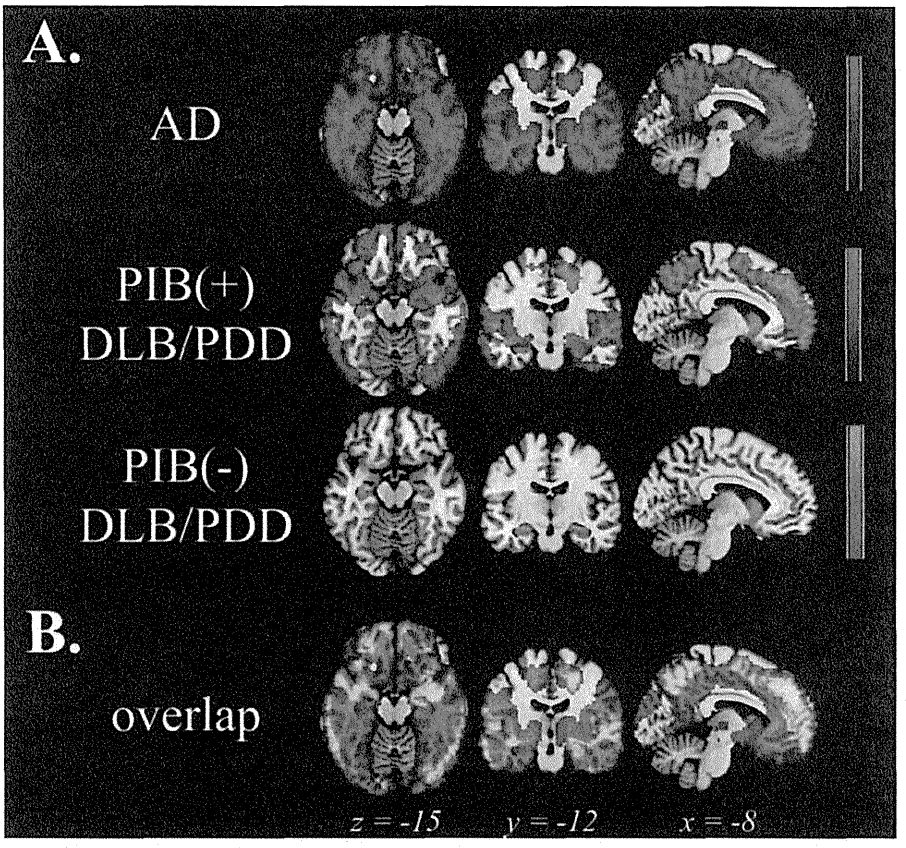

FIG. 2. Statistical parametric map of comparisons between three patient groups and controls in GMV. (**A**) Regions where a reduction in GMV was observed in AD, PIB(+) DLB/PDD, and PIB(−) DLB/PDD, compared to healthy controls (FDR corrected, $P < 0.05$, extent threshold > 400). (**B**) Overlap (yellow) of brain areas with significant atrophy in PIB(+) DLB/PDD (green) and AD (red) groups, compared to healthy controls.

as lateral temporal and parietal cortices, compared to HC subjects. Furthermore, DLB/PDD patients with high cortical PIB uptake showed parahippocampal atrophy similar to AD patients, as compared to DLB/PDD patients with low cortical PIB uptake. These results suggest that Aβ deposition is associated with AD-like atrophy in DLB/PDD patients.

This study provides some additional insight into previous MRI studies on DLB/PDD. Two such studies compared the patterns of cortical atrophy between DLB and PDD. Beyer et al. reported that gray-matter density was significantly decreased in several cortices, such as temporal, occipital, and parietal cortices, in DLB patients, compared to PDD patients,[21] whereas Burton et al. reported that no significant volumetric differences were observed between PDD and DLB patients.[22] The different results of the two studies could be explained by the difference in prevalence of subjects with high cortical Aβ deposition.

There have been several attempts to elucidate the role of Aβ deposition in the development of dementia in DLB/PDD. In a pathological study, PDD had significantly more AD-like neurofibrillary and Aβ plaque pathology than PD without dementia, suggesting that Aβ plays a role in the development of dementia in PDD.[23] Compta et al. reported that cortical Aβ scores were significantly correlated with MMSE scores in PDD.[24] Foster et al. reported that elevated PIB binding was associated with worse global cognitive impairment in participants with LB disorders, but was not related to any other clinical or neuropsychological features.[25] However, Rowe et al. reported that PIB binding did not correlate with dementia severity in AD and DLB.[26] In our study, PIB binding did not correlate with dementia severity or any other neuropsychological features in either AD or PIB(+) DLB/PDD patients. In some previous studies as well as in ours, PIB binding would have been underestimated, especially in cases with severe cortical atrophy, such as AD patients, because of the absence of atrophy correction. It was still unclear whether this lack of atrophy correction had any influence on the lack of relationship between PIB binding and neuropsychological data; however, these inconsistent correlations between cortical Aβ load and neuropsychological measures suggest that Aβ is not the sole pathological determinant of dementia in DLB/PDD, as in AD. In most DLB/PDD patients, cortical LBs are widespread and there is